Experimental and quantum chemical studies on corrosion inhibition effect of 6-bromo-2-oxo-1,2-dihydroquinoline-4-carboxylic acid on mild steel in HCl solution

Y. Filali Baba[1], H. Elmsellem[2]*, Y. Kandri Rodi[1]*, H. Steli[5], F. Ouazzani Chahdi[1], Y. Ouzidan[1], N. K. Sebbar[3], E. M. Essassi[3], F. El-Hajjaji[4] and B. Hammouti[2]

[1]*Laboratory of Applied Organic Chemistry, Faculty of Science and Technology, University Sidi Mohammed Ben Abdallah, Fez, Morocco*
[2] *Laboratoire de chimie analytique appliquée, matériaux et environnement (LC2AME), Faculté des Sciences, B.P. 717, 60000 Oujda, Morocco*
[3]*Laboratoire de Chimie Organique Hétérocyclique, URAC 21, Pôle de Compétences Pharmacochimie, Mohammed V University, Faculté des Sciences, Av. Ibn Battouta, BP 1014 Rabat, Morocco*
[4]*Laboratoire d'Ingénierie d'Electrochimie, Modélisation et d'Environnement (LIEME), Faculté des sciences/Université Sidi Mohammed Ben Abdellah, Fès, Maroc*
[5]*Laboratoire mécanique & énergétique, Faculté des Sciences, Université Mohammed Premier, Oujda, Maroc*

_____

ABSTRACT

6-bromo-2-oxo-1,2-dihydroquinoline-4-carboxylic acid (P2) as a new corrosion inhibitor was synthesized in the present work. The corrosion inhibition of P2 in hydrochloric acid for mild steel was evaluated by potentiodynamic polarization measurements, electrochemical impedance spectroscopy, weight loss measurements, and DFT. The results indicate that the P2 is mixed type inhibitor, and the adsorption of P2 on mild steel surface obeys Langmuir isotherm. In addition, the inhibition efficiency increases with increasing the concentration of inhibitor. Correlation between quantum chemical calculations and inhibition efficiency of the investigated compound is discussed using the Density Functional Theory method (DFT).

Keywords: corrosion inhibition, 6-bromo-2-oxo-1,2-dihydroquinoline-4-carboxylic acid, Corrosion, Weight loss, Electrochemical, DFT.

_____

INTRODUCTION

The Construction and synthesis of new heterocyclic compounds with multiple uses, has led us to a new quinolone class which has a broad spectrum of bactericidal activity [1-6]. Quinolone derivatives has become a famous popular class of antibiotics for use in a variety of infections [7]. Newer class of these synthesized molecules has been developed with a various spectrum of activity such as antifungal [8], antitumor [9]. Several classes of organic compounds like quinolones are widely used as corrosion inhibitors for metals in acid environments [10-12] (Scheme 1).
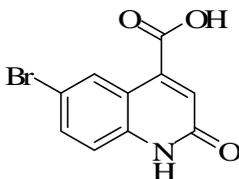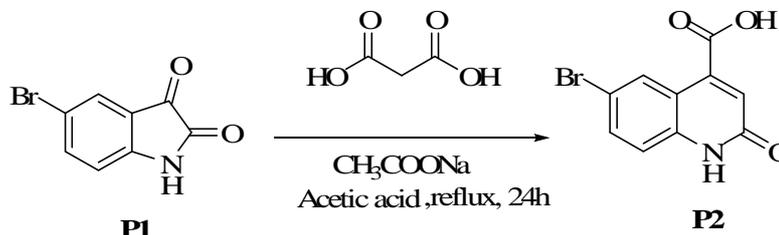

Scheme 1: 6-bromo-2-oxo-1,2-dihydroquinoline-4-carboxylic acid (P2)

_____

<div align="center">

MATERIALS AND METHODS

</div>

2.1. Synthesis of inhibitor
To a solution of 10 mmol of 5- bromo-isatin (P1) and 10 mmol of malonic acid in 30 ml of acetic acid was added 1 mmol of sodium acetate. The reaction mixture was refluxed for 24 hours. After cooling 100 ml of water-ice was added. The precipitate obtained was washed several times with ethanol. (**Scheme 2**):

<div align="center">

Scheme 2: Synthesis of 6- bromo-2-oxo-1,2-dihydroquinoline-4-carboxylic acid (P2)

</div>

The analytical and spectroscopic data are conforming to structure of compound formed.

(P2): Yield= 85 % ; **Mp:** 555K; **^{1}H NMR (300 MHz, DMSO-d6) :** 6.98 (s, 1H,C*H*) ; 7.30 (d,1H, J_{H-H}= 9 Hz, (C*H$_{arom}$*); 7.7 (dd, 1H, J_{H-H} = 9 Hz, J_{H-H} = 1.8 Hz (C*H$_{arom}$*); 8.42 (d, 1H, J_{H-H} = 1.8Hz, (C*H$_{arom}$*); 12.22(s, 1H, N*H*) ; 14.05 (s, 1 H, O*H*). **^{13}C NMR (75 MHz, DMSO-d6) :** 166.7 (*C*OOH), 161.2 (*C*=O), 139.6-139 (*C*q,*C*q), 133.8 (*CH$_{arom}$*), 128.7 (*CH$_{arom}$*), 125.9 (*CH*), 118.3 (*CH$_{arom}$*), 117.9 (*C*q). 114.5 (*CH$_{arom}$*). **Mass Spectrometry (DIC / NH$_3$)** :[MH]+ (m/z = 268)

2.2. Solutions
The aggressive solutions of 1.0 M HCl were prepared by dilution of an analytical grade 37% HCl with double distilled water. Inhibitor solutions with concentrations of 10^{-6} to 10^{-3} mol dm^{-3} were employed for inhibition studies and were prepared by dissolving the required amount of (**P2**) in 100 mL of 1 M HCl by stirring at room temperature. 100 mL of 1 M HCl without inhibitor was used as blank test solution.

2.3. Experimental techniques
2.3.1. Weight loss measurements
Coupons were cut into 1.5× 1.5 × 0.05 cm^3 dimensions having composition (0.09%P, 0.01 % Al, 0.38 % Si, 0.05 % Mn, 0.21 % C, 0.05 % S and Fe balance) used for weight loss measurements. Prior to all measurements, the exposed area was mechanically abraded with 180, 400, 800, 1000, 1200 grades of emery papers. The specimens are washed thoroughly with bidistilled water degreased and dried with ethanol. Gravimetric measurements are carried out in a double walled glass cell equipped with a thermostated cooling condenser. The solution volume is 50 cm^3. The immersion time for the weight loss is 6 h at (308±1) K. In order to get good reproducibility, experiments were carried out in duplicate. The average weight loss was obtained. The corrosion rate (*v*) is calculated using the following equation:

$$v = W / S.t \qquad (1)$$

Where: W is the average weight loss, S the total area, and t is immersion time. With the corrosion rate calculated, the inhibition efficiency (E$_w$) is determined as follows:

$$E_w \% = (V_0 - V/ V_0)*100 \qquad (2)$$

Where: **V$_0$** and **V** are, respectively, the values of corrosion rate with and without inhibitor.
2.3.2. Electrochemical tests
The electrochemical study was carried out using a potentiostat PGZ100 piloted by Voltamaster soft-ware. This potentiostat is connected to a cell with three electrode thermostats with double wall. A saturated calomel electrode (SCE) and platinum electrode were used as reference and auxiliary electrodes, respectively. Anodic and cathodic potentiodynamic polarization curves were plotted at a polarization scan rate of 0.5mV/s. Before all experiments, the potential was stabilized at free potential during 30 min. The polarisation curves are obtained from −800 mV to −200 mV at 308 K. The solution test is there after de-aerated by bubbling nitrogen. Inhibition efficiency (E$_p$%) is defined as Equation (3), where i$_{corr(0)}$ and i$_{corr(inh)}$ represent corrosion current density values without and with inhibitor, respectively.

<div align="center">

Scholar Research Library

</div>

$$E_p\% = (i_{corr(0)} - i_{corr(inh)} / i_{corr(0)})*100 \quad \textbf{(3)}$$

The electrochemical impedance spectroscopy (EIS) measurements are carried out with the electrochemical system, which included a digital potentiostat model Voltalab PGZ100 computer at E_{corr} after immersion in solution without bubbling. After the determination of steady-state current at a corrosion potential, sine wave voltage (10 mV) peak to peak, at frequencies between 100 kHz and 10 mHz are superimposed on the rest potential. Computer programs automatically controlled the measurements performed at rest potentials after 0.5 hour of exposure at 308 K. The impedance diagrams are given in the Nyquist representation. Inhibition efficiency ($E_R\%$) is estimated using the relation(4), where $R_{t(0)}$ and $R_{t(inh)}$ are the charge transfer resistance values in the absence and presence of inhibitor, respectively:

$$E_R\% = (R_{t(inh)} - R_{t(0)} / R_{t(inh)})*100 \quad \textbf{(4)}$$

2.4. Quantum chemical calculations
All the quantum chemical calculations have been carried out with Gaussian 09 programmed package [13, 14]. In our calculation we have used B3LYP, a hybrid functional of the DFT method, which consists of the Becke's three parameters; exact exchange functional B3 combined with the nonlocal gradient corrected correlation functional of Lee-Yang-Par (LYP) has been used along with 6-31G(dp) basis set. In the process of geometry optimization for the fully relaxed method, convergence of all the calculations has been confirmed by the absence of imaginary frequencies. The aim of our calculation is to calculate the following quantum chemical indices: the energy of highest occupied molecular orbital (E_{HOMO}), the energy of lowest unoccupied molecular orbital (E_{LUMO}), energy gap (ΔE), hardness (η), sotness (σ), electrophilicity index (ω), the fraction of electrons transferred (ΔN) from inhibitor molecule to the metal surface, and energy change when both processes occur, namely, and correlate these with the experimental observations.

The electronic populations as well as the Fukui indices and local nucleophilicities are computed using NPA (natural population analysis) [15–17]. Our objective, in this study, is to investigate computationally inhibitory action of quinoline derivative **P2** with chloridric acid in gas and in aqueous phase using B3LYP method with 6-31G(d,p) basis set.

➢ *Theory and computational details*
Theoretical study of benzothiazine derivative with chloridric acid as corrosion inhibitors was done by using the Density Functional Theory (DFT) with the B3LYP [18] /6-31G(d,p) method implemented in Gaussian 09 program package.

In this study, some molecular properties were calculated such as the frontier molecular orbital (HOMO and LUMO) energies, energy gap (E_{Gap}), charge distribution, electron affinity (A), ionization

Popular qualitative chemical concepts such as electronegativity [19, 20] (χ) and hardness [21] (η) have been provided with rigorous definitions within the purview of conceptual density functional theory(DFT) [22–24].

Using a finite difference method, working equations for the calculation of χ and η may be given as [22]:

$$\chi = \frac{I+A}{2} \ , \quad \chi = -\frac{1}{2}(E_{HOMO} + E_{LUMO}) \ (5)$$
$$\eta = \frac{I-A}{2} \ , \quad \eta = -\frac{1}{2}(E_{HOMO} - E_{LUMO}) \ (6)$$

Where I = $-E_{HOMO}$ and A= $-E_{LUMO}$ are the ionization potential and electron affinity respectively.
Local quantities such as Fukui function defined the reactivity/selectivity of a specific site in a molecule.
Using left and right derivatives with respect to the number of electrons, electrophilic and nucleophilic Fukui functions for a site k in a molecule can be defined [25].

$$f_k^+ = P_k(N+1) - P_k(N) \quad for\ nucleophilic\ attack \quad \textbf{(7)}$$
$$f_k^- = P_k(N) - P_k(N-1) \quad for\ electrphilic\ attack \quad \textbf{(8)}$$
$$f_k^+ = [P_k(N+1) - P_k(N-1)]/2 \quad for\ radical\ attack \quad \textbf{(9)}$$

where, $P_k(N)$, $P_k(N+1)$ and $P_k(N-1)$ are the natural populations for the atom k in the neutral, anionic and cationic species respectively.

The fraction of transferred electrons ΔN was calculated according to Pearson theory [26]. This parameter evaluates the electronic flow in a reaction of two systems with different electronegativity, in particular case; a metallic surface (Fe) and an inhibitor molecule. ΔN is given as follows:

$$\Delta N = \frac{\chi_{Fe} - \chi_{inh}}{2(\eta_{Fe} + \eta_{inh})} \quad (10)$$

Where χ_{Fe} and χ_{inh} denote the absolute electronegativity of an iron atom (Fe) and the inhibitor molecule, respectively; ηFe and ηinh denote the absolute hardness of Fe atom and the inhibitor molecule, respectively. In order to apply the eq. 10 in the present study, a theoretical value for the electronegativity of bulk iron was used $\chi_{Fe} = 7$ eV and a global hardness of $\eta_{Fe} = 0$, by assuming that for a metallic bulk I = A because they are softer than the neutral metallic atoms [26].

The electrophilicity has been introduced by Parr et al. [22], is a descriptor of reactivity that allows a quantitative classification of the global electrophilic nature of a compound within a relative scale. They have proposed the ω as a measure of energy lowering owing to maximal electron flow between donor and acceptor and ω is defined as follows.

$$\omega = \frac{\chi^2}{2\eta} \quad (11)$$

The Softness σ is defined as the inverse of the η [26]

$$\sigma = \frac{1}{\eta} \quad (12)$$

RESULTS AND DISCUSSION

3.1. Weight loss measurements

The weight loss method is beneficial for monitoring inhibition efficiency due to its simple usage and reliability. The effect of P2 addition at different concentration on mild steel in 1M HCl was studied by weight loss measurement at 308 K for 6 h immersion period.

Table 1. Corrosion parameters for mild steel in 1 M HCl in the presence and absence of different concentrations of P2 obtained from weight loss measurements at 308K

Inhibitors	Concentration (M)	ν (mg.cm^{-2}h^{-1})	E_w (%)	θ
1M HCl	---	0.82	---	---
P2	**10^{-6}**	0.35	57	0.57
	10^{-5}	0.23	72	0.72
	10^{-4}	0.12	85	0.85
	10^{-3}	0.09	89	0.89

At a given temperature, the inhibition efficiency (Ew %) of P2 increases with increasing inhibitor concentration to reach a maximum (89%) at a certain critical concentration (10^{-3}).

Beyond the critical concentration, the inhibition efficiency tends to decrease slightly and finally achieves steady state values. From the values of inhibition efficiency, it is evident that the corrosion inhibition may be due to adsorption of the P2 on the metal surface. The adsorption of the P2 on the metal surface makes a barrier for mass and charge transfers thus protecting the metal surface from corrosion.

3.2. Adsorption isotherm

The interaction between the metal surface and the organic molecules is expressed by adsorption isotherms. Adsorption of organic molecules on a metal surface is a substitution process between the water molecules at the metal surface and P2 in the electrolyte solution [27]. The adsorption of the inhibitor on the mild steel depends on the degree of surface coverage (θ). The degree of surface coverage (θ) at different concentrations of the inhibitors on the corrosion of mild steel was calculated from gravimetric results (Table 2). The best fit among the tested various isotherms was obtained with the use of the Langmuir adsorption isotherms (Figure 1), which may be expressed by the following equation:

$$\frac{C}{\theta} = \frac{1}{k} + C \quad (13)$$

Where C_{inh} is inhibitor concentration, and K_{ads} is equilibrium constant of adsorption.

The plots of C_{inh}/θ versus C_{inh} show the expected linear relationship for P2 in Figure 1. The K_{ads}, obtained from linear equation of the straight line is 3.49×10^5 for P2. The Langmuir isotherm indicates that one monolayer of P2 molecule is formed on the metal surface [28]. Based on the Langmuir isotherm, the standard free energy of adsorption ($\Delta G°_{ads}$) can be estimated by the following equation:

$$\Delta G_{ads} = -RT\ln(55,5K) \qquad \textbf{(14)}$$

Where R is the universal gas constant and T is the absolute temperature.
According to Eq.(14), $\Delta G°_{ads}$ was calculated as -42.94 kJ mol-1 at 308 K, which suggested that the adsorption of inhibitor molecules is merely physisorption and it may include a comprehensive adsorption (physical adsorption). However, the adsorption of inhibitor molecules on the metal surfaces accepted as completely physical phenomenon. In fact, there is no clear boundary between the physical and chemical adsorption.

Generally, the $\Delta G°ads$ values of -20 kJ/mol or less negative are associated with an electrostatic interaction between charged molecules and charged metal surface (physisorption); those of -40 kJ/moL or more negative involves charge sharing or transfer from the inhibitor molecules to the metal surface to form a coordinate covalent bond (chemisorption) [29]. In the present study, the obtained values of $\Delta G°$ ads surrounded -40 kJ/moL indicating that the adsorption mechanism of the P2 tested on mild steel in HCl solution (1M) was typical of physical adsorption (**Figure 1**).
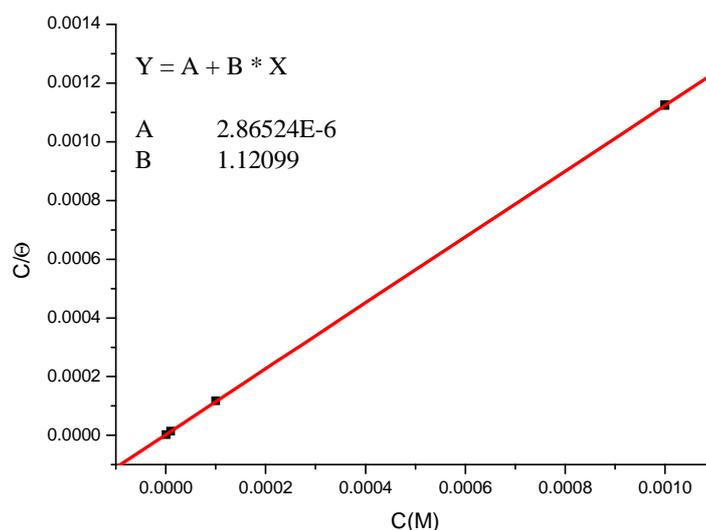

Figure 1. Langmuir adsorption isotherm for P2 on the mild steel surface

3.3. Tafel extrapolation
Polarization measurements have been carried out in order to gain knowledge concerning the kinetics of the anodic and cathodic reactions. Potentiodynamic curves are obtained in the presence and absence of the studied inhibitor P2, after pre-polarizing the electrode at its E_{corr} for 30 min, thereafter pre-polarized at -800 mV for 10 min. After this scan, the potential was swept stepwise from the most cathodic potential to the anodic direction. The effect of rise concentration of P2 on the anodic and cathodic polarisation curves of steel in 1 M HCl at 308 K is presented in Figure 2. Various corrosion parameters such as corrosion current densities (I_{corr}), corrosion potentials (E_{corr}), cathodic Tafel slopes (βc), degree of surfaces coverage (θ) and inhibition efficiencies Ep%, obtained from polarization measurements are listed in Table 2.
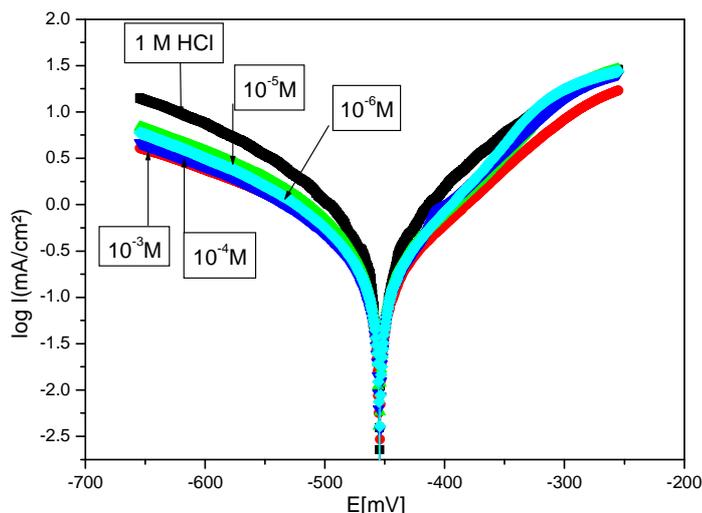
132

Figure 2. Polarisation curves of mild steel in 1M HCl at different concentrations of P2

Table 2. Values of electrochemical parameters evaluated from the cathodic current-voltage characteristics for the system electrode/1 M HCl with and without added inhibitor at 308 K

Inhibitor	Concentration (M)	Ecorr (mV/SCE)	Icorr ($\mu A/cm^2$)	βc (V/dec)	E$_p$ (%)
HCl 1M	--	-459	1381	-0.294	--
P2	10^{-6}	-457	671	-0.294	51
	10^{-5}	-459	378	-0.297	73
	10^{-4}	-444	179	-0.299	87
	10^{-3}	-451	135	-0.295	90

From the recorded results, we can conclude that in all cases, addition of the studied compound induced a marked decrease in the cathodic and a slight decrease in the anodic current densities. Accordingly, this inhibitor P2 affects greatly the hydrogen reaction discharge and slightly affects the mild steel dissolution processes. The hydrogen evolution reaction is under activation control since the cathodic portions rise to Tafel lines. The fact that cathodic process slow down can be due to the covering of the surface with monolayer of the tested molecule due to the adsorbed inhibitor on the mild steel surface then reducing the electrolyte infiltration to the interface.

3.4. Electrochemical impedance spectroscopy measurements
The corrosion behaviour of mild steel, in acidic solution in the presence of P2 at different concentrations was investigated by EIS measurements at 308K. As observed, the Nyquist plots contain a depressed semi-circle with the centre below the real X-axis, which is size increased by increasing the inhibitor concentrations, indicating that the corrosion is mainly a charge transfer process [30] and the formed inhibitive film was strengthened by the addition of P2. The depressed semi-circle is the characteristic of solid electrodes and often refers to the frequency dispersion which arises due to the roughness and other in homogeneities of the surface. It is worth noting that the change in concentration of P2 did not alter the style of the impedance curves, suggesting a similar mechanism of the inhibition is involved.

The equivalent circuit model employed for this system is as previously reported by fitting with Zview program [31] is showed in the in Figure 3. Nyquist plots of steel in inhibited and uninhibited acidic solutions containing various concentrations of P2 are shown in Figure 3. The charge-transfer resistance (R_t) values are calculated from the difference in impedance at lower and higher frequencies. To obtain the double layer capacitance (C_{dl}) the frequency at which the imaginary component of the impedance is maximal ($-Z_{max}$) is found as represented in equation 15 [32].

$$C_{dl} = \frac{1}{\omega . R_t} \qquad \text{Where} \qquad w = 2\Pi f_{max} \quad \textbf{(15)}$$
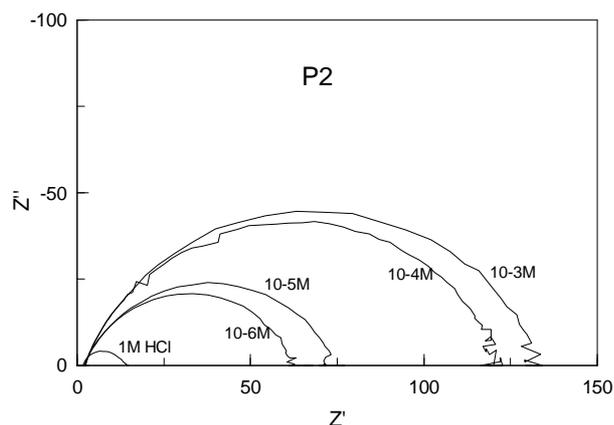
133

_____

Figure 3. Bode and phase plots of mild steel in 1.0 M HCl and in the presence different concentrations of P2 at 308 K

Table 3. Electrochemical parameters for mild steel in 1 M HCl without and with different concentrations of (P2) at 308K

Concentration (M) / Prameters	1M HCl	10^{-6}	10^{-5}	10^{-4}	10^{-3}
Real Center	9.25	32.254	37.748	61.778	67.882
Imag. Center	1.62	11.454	14.269	21.216	25.948
Diameter	15.13	64.569	76.649	125.95	141.54
Deviation	0.15	0.3781	0.65741	1.0033	0.52517
Low Intercept R_s ($\Omega.cm^2$)	1.86	2.0696	2.1789	2.4851	2.0406
High Intercept R_t ($\Omega.cm^2$)	16.64	62.439	73.317	121.07	133.72
Depression Angle	12.42	20.78	21.859	19.688	21.509
ω_{max} (rad s^{-1})	929.60	265.55	251.02	139.142	138.79
Estimated R_t($\Omega.cm^2$)	14.78	60.369	71.138	118.064	131.68
Estimated C_{dl}(F.cm^{-2})	7.11 10^{-5}	5.83 10^{-5}	5.19 10^{-5}	5.11 10^{-5}	5.09 10^{-5}
E_R(%)	--	76	79	86	89

Table 3 shows the impedance parameters obtained by line fitting to the semicircle. The charge transfer resistance (R_t) increases with the inhibitor concentration. Also, the double layer capacitance (C_{dl}) decreases with increase in the concentration of the inhibitor. This decrease is due to the adsorption of the inhibitor at the metal surface causing a change of the double layer structure [33-35].
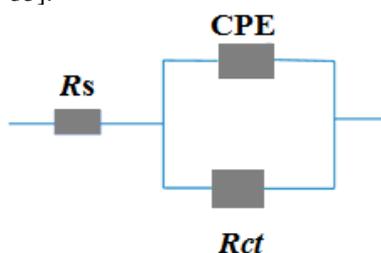

Figure 4. Equivalent circuit model used to fit the impedance spectra

3.5. Theoretical study
3.5.1. Quantum chemical calculations
In the last few years, the FMOs (HOMO and LUMO) are widely used for describing chemical reactivity. The HOMO containing electrons, represents the ability (E_{HOMO}) to donate an electron, whereas, LUMO haven't not electrons, as an electron acceptor represents the ability (E_{LUMO}) to obtain an electron. The energy gap between HOMO and LUMO determines the kinetic stability, chemical reactivity, optical polarizability and chemical hardness–softness of a compound [36]. In this paper, we calculated the HOMO and LUMO orbital energies by using B3LYP method with 6-31G(d,p). All other calculations were performed using the results with some assumptions. The higher values of E_{HOMO} indicate an increase for the electron donor and this means a better inhibitory activity with increasing adsorption of the inhibitor on a metal surface, whereas E_{LUMO} indicates the ability to accept electron of the molecule. The adsorption ability of the inhibitor to the metal surface increases with increasing of E_{HOMO} and decreasing of E_{LUMO}.

High ionization energy (I= 6.67 eV, I= 3.46 eV in gas and aqueous phases respectively) indicates high stability [37-39], the number of electrons transferred (ΔN) was also calculated and tabulated in Table 4. The number of electrons

134

_____

transferred (ΔN) was also calculated and tabulated in Table 5. The ΔN(gas) < 3.6 and ΔN(aqueous) < 3.6 indicates the tendency of a molecule to donate electrons to the metal surface [40, 41].

Table 4. Quantum chemical descriptors of the studied inhibitor at B3LYP/6-31G(d,p) in gas, G and aqueous, A phases

| Prameters	Phase	
	Gas	Aqueous
Total Energy *TE* (eV)	-88074.8	-88075.2
E_{HOMO} (eV)	-6.6735	-3.4576
E_{LUMO} (eV)	-0.4286	-1.3676
Gap *ΔE* (eV)	6.2450	2.0900
Dipole moment *μ* (Debye)	0.7808	1.2186
Ionisation potential *I* (eV)	6.6735	3.4576
Electron affinity *A*	0.4286	1.3676
Electronegativity *χ*	3.5510	2.4126
Hardness *η*	3.1225	1.0450
Electrophilicity index *ω*	2.0192	2.7849
Softness *σ*	0.3203	0.9569
Fractions of electron transferred *ΔN*	0.5523	2.1949

The calculated values of the f_k^+ for all inhibitors are mostly localized on the quinoline ring. Namely C_8, C_{12}, O_{14} and O_{17}, indicating that the quinoline ring will probably be the favorite site for nucleophilic attacks.

The results also show that O_{14} atom is suitable site to undergo both nucleophilic and electrophilic attacks, probably allowing them to adsorb easily and strongly on the mild steel surface.

Table 5. Pertinent natural populations and Fukui functions of the studied inhibitors calculated at B3LYP/6-31G(d,p) in gas, G and aqueous, A phases

Atom k	Phase	P(N)	P(N+1)	P(N-1)	f_k^+	f_k^-	f_k^0
C_8	G	6,10804	6,09713	6,22569	0,0109	0,1177	0,0643
	A	6,10525	6,09129	6,2279	0,014	0,1227	0,0683
C_{12}	G	6,24256	6,19122	6,38301	0,0513	0,1405	0,0959
	A	6,24337	6,38632	8,5549	0,0527	0,143	0,0978
O_{14}	G	8,60369	8,43102	8,69769	0,1727	0,094	0,1333
	A	8,64631	8,49089	8,73376	0,1554	0,0875	0,1214
O_{17}	G	8,5919	8,56706	8,6903	0,0248	0,0984	0,0616
	A	8,61253	8,59695	8,71552	0,0156	0,103	0,0593

The final optimized geometries of P2 in gas and aqueous, selected valence bond angle and dihedral angles and bond lengths are given in Figure 5.

P2 Gas phase   **P2 Aqueous phase**
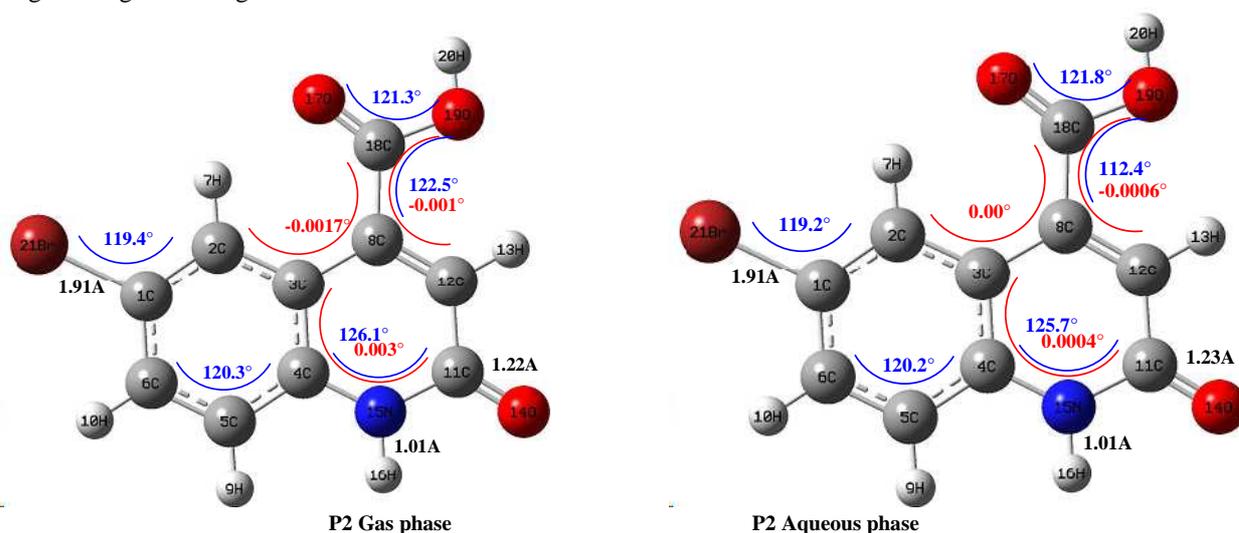
Figure 5. Optimized molecular structures, selected dihedral angles (red), valence bond angle (blue) and bond lengths (black) of the studied inhibitors calculated in gas and aqueous phases at B3LYP/6-31G(d,p) level of P2

After the analysis of the theoretical results obtained, we can say that the molecule **P2** have a non-planar structure.

_____

Table 6 : The HOMO and the LUMO electrons density distributions of the studied inhibitors computed at B3LYP/6-31G (d,p) level in gas and aqueous phases

	P2 Gas phase	**P2** Aqueous phase
HOMO		
LUMO		
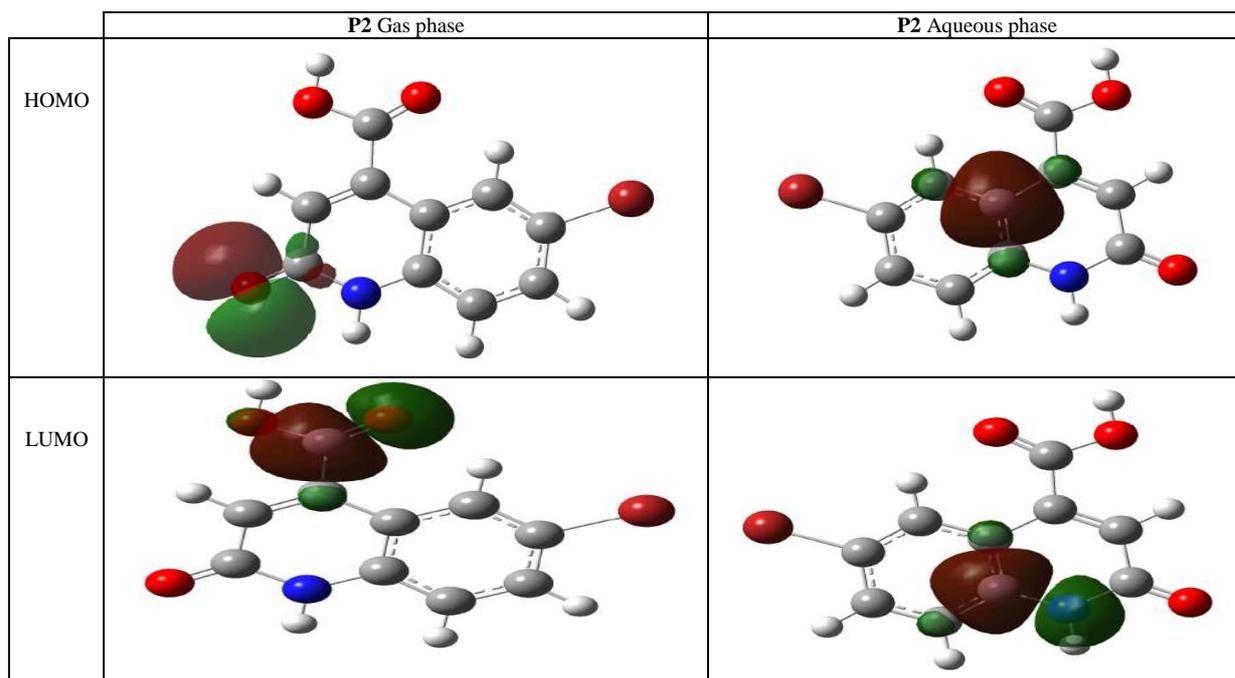
The inhibition efficiency afforded by the quinoline derivative P2 may be attributed to the presence of electron rich O.

CONCLUSION

The following results can be plotted from this work:

1) The corrosion rate of mild steel in 1M HCl, decreases upon the addition of the minimal concentration of P2 and inhibition efficiency increases with increasing P2 concentration.

2) The P2 acts as a mixed type inhibitor; it suppresses both anodic and cathodic reactions.

3) Inhibition is because of adsorption of the inhibitor molecules on the steel surface, thus blocking its active sites. Adsorption of the inhibitor P2 fits a modified Langmuir isotherm model.

4) Theoretical calculations (quantum chemical) are in good agreement with results obtained from electrochemical study and structure–corrosion protection relationships, which also confirm that the adsorption centre is N atom.

REFERENCES

[1] J.J. Pocidalo, *éd. Arnette, Paris*, **1985**.

[2] C. Spinorin, *Ann. Rev. Microbiol*, **1989**, 43,601.

[3] E. E. Ebenso, N. O. Eddy, A. O. Odiongenyi, *Portugaliae Electrochimica. Acta*,**2009**, 27(1) ,13.

[4] R. Khunt, N. Datta, F. Bharmal, A. R. Rarikh, *J. Ind. Chem. Soc*, **2001**, 78, 47.

[5] N.O. Eddy., S.A. Odoemelam , *Adv. Nat. & Appl. Sci,***2008** , 2(1),35.

[6] X. Zhang, *Journal of Infectious Diseases*, **2000**,181, 670.

[7] A. Naeem, *Molecules*, **2016**, 21, 268.

[8] A. Korolhovas, J. H. Burckhaltre, *éd. WileyInterscience Pub., New york*, **1983**, 404.

[9] H. Abe, *Organic. Letters*, **2013**, 15(9), 2127.

[10] H.Elmsellem, A.Aouniti, Y. Toubi, H. Steli, M. Elazzouzi, S. Radi, B. Elmahi, Y. El Ouadi, A. Chetouani, B. Hammouti, *Der Pharma Chemica*, **2015**, 7(7), 353-364.

[11] H Elmsellem., H. Bendaha, A. Aouniti, A. Chetouani, M. Mimouni, A. Bouyanzer, *Mor. J. Chem*, **2014**, 2 (1), 1-9.

[12] H. Elmsellem, A. Elyoussfi, H. Steli, N. K. Sebbar, E. M. Essassi, M. Dahmani, Y. El Ouadi, A. Aouniti, B. El Mahi, B. Hammouti, *Der Pharma Chemica*, **2016**, 8(1), 248-256.

[13] M.J.Frisch, G.W.Trucks, H.B.Schlegeletal, *Gaussian 09, Revision A.1, Gaussian, Inc., Wallingford, Conn, USA*, **2009**.

[14] H. Elmsellem, M. H. Youssouf, A. Aouniti, T. Ben Hadd, A. Chetouani, B. Hammouti, *Russian, Journal of Applied Chemistry*, **2014**,87(6), 744–753.

[15] J. Li, H. Li, M. Jakobsson, S. Li, P. Sjodin, M. Lascoux, *Mol. Ecol*, **2012**, 21, 28.

[16] M. Y. Hjouji, M. Djedid, H. Elmsellem, Y. Kandri Rodi, M. Benalia, H. Steli, Y. Ouzidan, F. Ouazzani Chahdi, E. M. Essassi, B. Hammouti, *Der Pharma Chemica*, **2016**, 8(4), 85-95.

[17] H. Elmsellem, T. Harit, A. Aouniti, F.Malek, A. Chetouani, B.Hammouti, *Protection of Metals and Physical Chemistry of Surfaces*, A, **2015**, 51(5), 873–884.

[18] K. Efil, Y. Bekdemir, *Canadian Chemical Transactions*, **2015**, 3(1), 85.

[19] L.Pauling, *3rd edn. Cornell University Press, Ithaca*, **1960**.

[20] K.D. Sen, C. *Jorgenson*, *Springer, Berlin,* **1987**, 66.

[21] K.D. Sen, D.M.P. Mingos, *Springer, Berlin*, **1993**, 80.

[22] R.G. Parr, W. Yang, *Oxford University Press, Oxford*, **1989**.

[23] P.Geerlings, F. Proft, W. Langenaeker, *Chem. Rev,***2003**,103, 1793.

[24] H.Chermette, *Comput J.Chem*, **1999**, 20,129.

[25] R.K.Roy, S.Pal, K.Hirao, *J. Chem. Phys*, **1999**, 110, 8236.

[26] R.G.Pearson, *Inorg. Chem*, **1988**, 27, 734.

[27] N. K. Sebbar, H. Elmsellem, M. Boudalia, S. lahmidi, A. Belleaouchou , A. Guenbour, E. M. Essassi, H. Steli, A. Aouniti, *J. Mater. Environ. Sci,* **2015**, 6 (11), 3034-3044.

[28] H. Elmsellem, A. Aouniti, M. Khoutoul, A. Chetouani, B. Hammouti, N. Benchat, R. Touzani, M. Elazzouzi, *Journal of Chemical and Pharmaceutical Research*, **2014**, 6(4), 1216-1224.

[29] H. Elmsellem, H. Nacer, F. Halaimia, A. Aouniti, I. Lakehal, A. Chetouani, S. S. Al-Deyab, I. Warad, R.Touzani, B. Hammouti, *Int. J. Electrochem. Sci*, **2014**, 9, 5328.

[30] H. Elmsellem, N. Basbas, A. Chetouani, A. Aouniti, S. Radi, M. Messali, B. Hammouti, *Portugaliae. Electrochimica. Acta*, 2014, 2, 77.

[31] A. Aouniti, H. Elmsellem, S.Tighadouini, M. Elazzouzi, S. Radi, A. Chetouani, B. Hammouti, A. Zarrouk, *Journal of Taibah University for Science*, **2015**, http://dx.doi.org/10.1016/j.jtusci.2015.11.008.

[32] H. Elmsellem, K. Karrouchi, A. Aouniti, B. Hammouti, S. Radi, J. Taoufik, M. Ansar, M. Dahmani, H. Steli, B. El Mahi, *Der Pharma Chemica*, **2015**, 7(10), 237-245.

[33] Y. Filali Baba, H. Elmsellem, Y. Kandri Rodi, H. Steli, C. AD, Y. Ouzidan, F. Ouazzani Chahdi, N. K. Sebbar, E. M. Essassi, B. Hammouti, *Der Pharma Chemica*, **2016**, 8(4), 159-169.

[34] M. Ellouz, H. Elmsellem, N. K. Sebbar, H. Steli, K. Al Mamari, A. Nadeem, Y. Ouzidan, E. M. Essassi, I. Abdel-Rahaman, P. Hristov, *J. Mater. Environ. Sci*, **2016**,7(7), 2482-2497.

[35] P. Udhayakala, T. V. Rajendiran, S. Gunasekaran, *Journal of Chemical, Biological and Physical Sciences A*, **2012**, 2(3),1151–1165.

[36] M. Govindarajan, M. Karabacak, *Spectrochim Acta Part A Mol Biomol Spectrosc*, **2012**, 85, 251–260.

[37] M. Sikine, Y. Kandri Rodi, H. Elmsellem, O. Krim, H. Steli, Y. Ouzidan, A. Kandri Rodi, F. Ouazzani Chahdi, N. K. Sebbar, E. M. Essassi, *J. Mater. Environ. Sci*, **2016**, 7 (4), 1386-1395.

[38] M. Y. Hjouji, M. Djedid, H. Elmsellem, Y.Kandri Rodi, Y. Ouzidan, F. Ouazzani Chahdi, N. K. Sebbar, E. M. Essassi, I. Abdel-Rahman, B. Hammouti, *J. Mater. Environ. Sci*, **2016**, 7(4), 1425-1435.

[39] I. Chakib, H. Elmsellem, N. K. Sebbar, S. Lahmidi, A. Nadeem, E. M. Essassi, Y. Ouzidan, I. Abdel-Rahman, F. Bentiss, B. Hammouti., *J. Mater. Environ. Sci*, **2016**, 7(6), 1866-1881.

[40] I. Lukovits, E. Kalman, F. Zucchi, *Corrosion*, **2001**, 57, 3-7.

[41] Y. Filali Baba, H. Elmsellem, Y. Kandri Rodi, H. Steli, F. Ouazzani Chahdi, Y. Ouzidan, N. K. Sebbar, E. M. Essassi, K. Cherrak., *J. Mater. Environ. Sci,* **2016**,7 (7), 2424-2434.